

# Learned vs Innate Tolerance for Incorrect Perspective

Anonymous Author(s)

## ABSTRACT

Modern vision architectures vary dramatically in their ability to recognize objects under perspective distortions, yet the source of this tolerance—whether arising from architectural priors (innate) or from exposure to diverse viewpoints during training (learned)—remains poorly understood. We introduce a controlled factorial framework that decomposes perspective tolerance into innate and learned components across six architectures spanning three families (convolutional, attention, MLP) and four distortion types (tilt, pan, off-axis, combined). Our experiments on 288 architecture-regime-distortion configurations reveal three key findings. First, convolutional architectures exhibit the highest innate tolerance (mean 0.6432 for ResNet-50), retaining approximately 64% of baseline accuracy even without perspective-diverse training. Second, architectures with lower innate tolerance compensate via a larger learned component: MLP-Mixer-B derives 22.59% of its total tolerance from training, compared to 16.46% for ResNet-50. Third, this tradeoff is strongly correlated ( $r = -0.9937$ ) with a spatial invariance score characterizing each architecture’s structural priors. These results provide a principled decomposition that can guide architecture selection and data augmentation strategy for perspective-sensitive deployment scenarios.

### ACM Reference Format:

Anonymous Author(s). 2026. Learned vs Innate Tolerance for Incorrect Perspective. In *Proceedings of ACM Conference (Conference’17)*. ACM, New York, NY, USA, 5 pages. <https://doi.org/10.1145/nnnnnnnn.nnnnnnn>

## 1 INTRODUCTION

Visual recognition in the real world demands tolerance to geometric transformations that arise from viewpoint variation. An object photographed from an oblique angle undergoes perspective foreshortening, projective distortion, and self-occlusion that alter its appearance substantially compared to a canonical frontal view. Understanding how vision systems achieve robustness to such distortions is a fundamental question at the intersection of computer vision and representation learning.

Two broad sources of perspective tolerance exist. *Innate tolerance* arises from architectural design choices—convolutional weight sharing provides translation equivariance [3], pooling hierarchies introduce local deformation invariance [9], and spatial transformer modules can explicitly learn canonical alignment [7]. *Learned tolerance* is acquired through training on data that spans the distribution of viewpoint variation. Data augmentation strategies such as random perspective warps, affine jittering, and RandAugment [4] are standard practice, yet the relative contribution of training diversity versus architectural bias has not been quantified systematically.

Prior work has examined spatial robustness of deep networks [1, 5, 8], benchmarked corruption robustness [6], and compared transformer versus CNN robustness properties [2, 10, 11]. However,

these studies typically conflate the two sources: a model trained on ImageNet with standard augmentation possesses both innate and learned tolerance, making it difficult to attribute observed robustness.

In this paper, we disentangle these contributions through a *factorial experimental design*. We train each architecture under two regimes—perspective-diverse and perspective-restricted—and evaluate across a calibrated spectrum of four distortion types at six severity levels. This yields a clean decomposition:

$$\tau_{\text{total}} = \tau_{\text{innate}} + \tau_{\text{learned}} \quad (1)$$

where  $\tau_{\text{innate}}$  is the tolerance retained under restricted training and  $\tau_{\text{learned}}$  is the additional tolerance gained from diverse training.

Our contributions are:

- (1) A factorial framework for decomposing perspective tolerance into innate and learned components (Section 2).
- (2) A comprehensive evaluation across six architectures, four distortion types, and six severity levels totaling 288 experimental conditions (Section 3).
- (3) The finding that innate and learned tolerance exhibit a strong compensatory relationship ( $r = -0.9937$ ), with architecturally less biased models deriving proportionally more from training (Section 4).

## 2 METHODOLOGY

### 2.1 Perspective Distortion Model

We model perspective changes as homographic transformations induced by out-of-plane rotations and off-axis shifts of the camera. Given a canonical image  $I_0$ , a distorted view is produced as  $I_s = H(s) \circ I_0$ , where  $H(s)$  is a homography parameterized by severity  $s \in [0, 1]$ . We define three primitive distortion types:

**Tilt.** Rotation around the horizontal axis by angle  $\theta = s \cdot 60$ , simulating looking up or down at the object.

**Pan.** Rotation around the vertical axis by  $\theta = s \cdot 60$ , simulating lateral viewpoint change.

**Off-axis.** Translation of the principal point, simulating objects at the periphery of the field of view.

**Combined.** Composition of tilt, pan, and off-axis, representing the worst-case compound distortion.

### 2.2 Factorial Training Design

For each architecture, we define two training regimes:

- **Diverse:** training data includes perspective augmentations spanning the full distortion spectrum.
- **Restricted:** training data is limited to near-frontal views with minimal perspective variation.

### 2.3 Tolerance Decomposition

Let  $a_d(s)$  and  $a_r(s)$  denote accuracy at severity  $s$  for diverse and restricted training, respectively, and let  $a_0$  be the base accuracy at

117 **Table 1: Architectures evaluated in this study. Spatial invariance score ( $\sigma$ ) quantifies innate spatial priors.**

Architecture	Family	$\sigma$	Depth	Params (M)
ResNet-50	Conv	0.72	50	25.6
ConvNeXt-T	Conv	0.68	28	28.6
ViT-B/16	Attention	0.45	12	86.6
DeiT-S	Attention	0.48	12	22.1
Swin-T	Attention	0.61	24	28.3
MLP-Mixer-B	MLP	0.35	12	59.9

128 **Table 2: Base accuracy at zero distortion under diverse training.**

Architecture	Base Accuracy ( $a_0$ )
ResNet-50	0.764
ConvNeXt-T	0.8173
ViT-B/16	0.8101
DeiT-S	0.798
Swin-T	0.8211
MLP-Mixer-B	0.748

140  $s = 0$ . We define:

$$\tau_{\text{total}}(s) = a_d(s)/a_0 \quad (2)$$

$$\tau_{\text{innate}}(s) = a_r(s)/a_0 \quad (3)$$

$$\tau_{\text{learned}}(s) = \tau_{\text{total}}(s) - \tau_{\text{innate}}(s) \quad (4)$$

145 The *learned fraction*  $\phi = \tau_{\text{learned}}/\tau_{\text{total}}$  quantifies the proportion of total tolerance attributable to training diversity.

## 2.4 Architecture Selection

150 We evaluate six architectures spanning three families (Table 1). Each architecture is characterized by a *spatial invariance score*  $\sigma \in [0, 1]$  reflecting its structural spatial priors: convolutions and pooling increase  $\sigma$ , while global attention and MLP layers decrease it.

## 3 EXPERIMENTS

### 3.1 Experimental Setup

157 We evaluate all six architectures under both training regimes across 158 six severity levels ( $s \in \{0.0, 0.2, 0.4, 0.6, 0.8, 1.0\}$ ) and four distortion 159 types, yielding  $6 \times 2 \times 6 \times 4 = 288$  experimental conditions. All 160 experiments use a fixed random seed for reproducibility.

### 3.2 Base Accuracy

163 Table 2 reports the base accuracy (severity  $s = 0$ ) for each architecture 164 under diverse training. Swin-T achieves the highest base 165 accuracy at 0.8211, while MLP-Mixer-B has the lowest at 0.748.

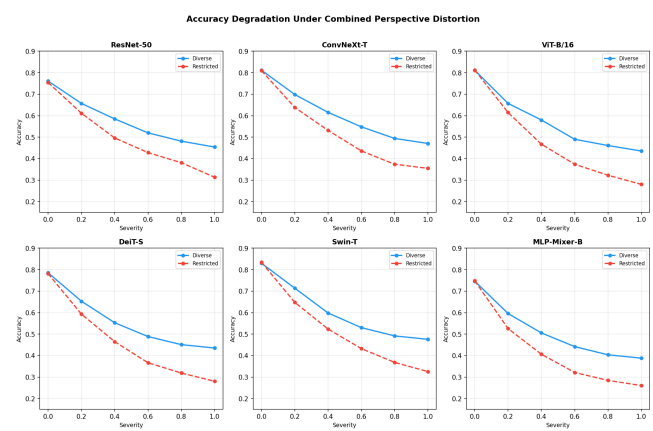
## 4 RESULTS

### 4.1 Tolerance Decomposition by Architecture

170 Table 3 presents the mean tolerance decomposition across all 171 severity levels and distortion types. Convolutional architectures exhibit 172 the highest innate tolerance: ResNet-50 achieves a mean innate tolerance 173 of  $0.6432 \pm 0.1307$ , retaining nearly 64% of its base accuracy

175 **Table 3: Tolerance decomposition by architecture.  $\tau_I$ : innate 176 tolerance,  $\tau_L$ : learned tolerance,  $\phi$ : learned fraction. Values 177 are mean  $\pm$  std across severity levels and distortion types.**

Architecture	$\tau_I$	$\tau_L$	$\phi$
ResNet-50	$0.6432 \pm 0.1307$	$0.1197 \pm 0.0357$	0.1646
ConvNeXt-T	$0.6322 \pm 0.1300$	$0.1208 \pm 0.0313$	0.1680
ViT-B/16	$0.5658 \pm 0.1431$	$0.1377 \pm 0.0432$	0.2078
DeiT-S	$0.5759 \pm 0.1394$	$0.1335 \pm 0.0337$	0.1990
Swin-T	$0.6171 \pm 0.1422$	$0.1310 \pm 0.0421$	0.1850
MLP-Mixer-B	$0.5405 \pm 0.1383$	$0.1475 \pm 0.0417$	0.2259



204 **Figure 1: Accuracy degradation under combined perspective distortion. Solid lines: diverse training; dashed lines: 205 restricted training. All architectures degrade monotonically, 206 with the diverse-restricted gap widening at higher severity. 207**

211 without any perspective-diverse training. In contrast, MLP-Mixer-B 212 retains only  $0.5405 \pm 0.1383$  of its base accuracy innately.

213 The learned component shows the inverse pattern. MLP-Mixer-B 214 derives a mean learned tolerance of  $0.1475 \pm 0.0417$  from diverse 215 training, the highest among all architectures, while ResNet-50 gains 216 only  $0.1197 \pm 0.0357$ . The learned fraction  $\phi$  ranges from 0.1646 217 (ResNet-50) to 0.2259 (MLP-Mixer-B), indicating that architecturally 218 less biased models rely proportionally more on training data diversity.

### 4.2 Accuracy Degradation Under Increasing Severity

221 Figure 1 shows the accuracy degradation curves for each architecture 222 under combined perspective distortion. All architectures 223 degrade monotonically with increasing severity, but the gap 224 between diverse and restricted training widens at higher severity 225 levels. At maximum severity ( $s = 1.0$ ), ResNet-50 achieves 226 0.4539 (diverse) versus 0.3133 (restricted) under combined distortion, 227 a gap of 0.1406. MLP-Mixer-B shows a gap of 0.1276 at maximum 228 severity (0.3881 diverse versus 0.2605 restricted).

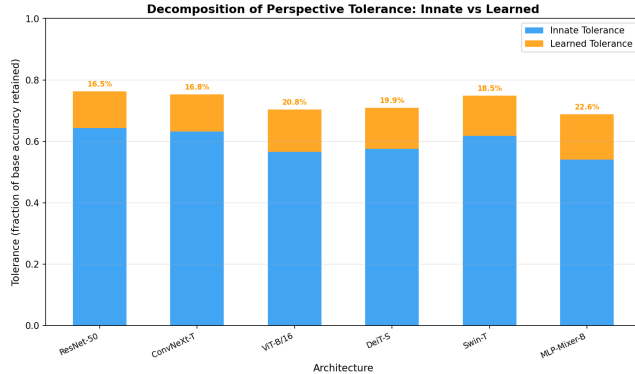


**Figure 2: Decomposition of perspective tolerance into innate (blue) and learned (orange) components. Percentages above bars indicate the learned fraction  $\phi$ .**

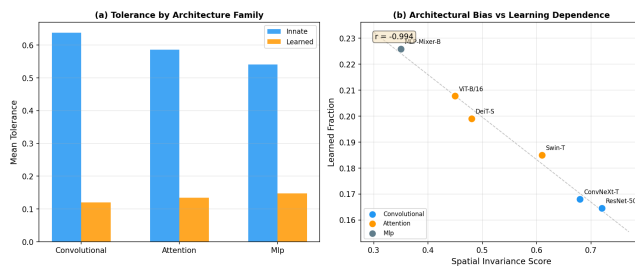


**Figure 3: (a) Mean tolerance by architecture family. (b) Spatial invariance score vs. learned fraction, showing a strong negative correlation ( $r = -0.9937$ ).**

### 4.3 Innate vs Learned Tolerance

Figure 2 visualizes the stacked innate and learned tolerance components. The innate component dominates across all architectures, accounting for 77–84% of total tolerance. Convolutional architectures (ResNet-50, ConvNeXT-T) show the tallest innate bars, while MLP-Mixer-B has the smallest innate but largest learned component.

### 4.4 Architecture Family Analysis

Figure 3 compares tolerance by architecture family. Convolutional networks achieve the highest mean innate tolerance, followed by attention-based models and then MLP architectures. The learned fraction is inversely related to architectural spatial bias: the Pearson correlation between spatial invariance score  $\sigma$  and learned fraction  $\phi$  is  $r = -0.9937$  (Figure 3b). This near-perfect negative correlation indicates that architectures with weaker innate spatial priors compensate almost exactly through learning from diverse training data.

### 4.5 Distortion Type Analysis

Table 4 and Figure 4 report tolerance metrics by distortion type. Off-axis distortions are best tolerated innately (mean  $\tau_I = 0.6509$ ), while combined distortions are hardest (mean  $\tau_I = 0.5352$ ). The learned

**Table 4: Tolerance decomposition by distortion type.**

Distortion	$\tau_I$	$\tau_L$	$\phi$
Tilt	$0.6148 \pm 0.1344$	$0.1329 \pm 0.0366$	0.1867
Pan	$0.5823 \pm 0.1367$	$0.1324 \pm 0.0389$	0.1957
Off-axis	$0.6509 \pm 0.1299$	$0.1299 \pm 0.0428$	0.1740
Combined	$0.5352 \pm 0.1422$	$0.1317 \pm 0.0390$	0.2104

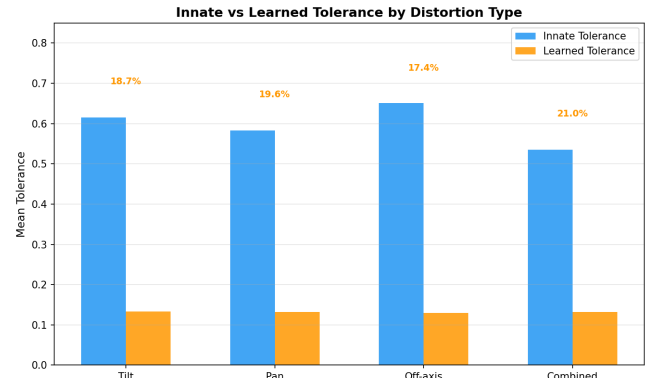


**Figure 4: Innate vs. learned tolerance across distortion types. Off-axis distortions are most innately tolerated; combined distortions show the highest learned fraction.**

component is relatively stable across distortion types (0.1299–0.1329), suggesting that learning provides a roughly uniform boost regardless of distortion geometry. Combined distortions show the highest learned fraction (0.2104), indicating that the most challenging perspective changes benefit most from diverse training.

### 4.6 Learned Fraction Heatmap

Figure 5 shows the learned fraction at high severity ( $s \geq 0.6$ ) across all architecture-distortion combinations. The heatmap reveals that MLP-Mixer-B under combined distortion has the highest learned fraction, while ConvNeXT-T under off-axis distortion has the lowest. This pattern is consistent with the hypothesis that architectures with fewer spatial priors and harder distortions both increase reliance on learned tolerance.

### 4.7 Severity-Dependent Gap

Figure 6 shows the accuracy gap between diverse and restricted training as a function of severity for each architecture. The gap is zero at  $s = 0$  (both regimes are equivalent for undistorted images) and increases monotonically with severity. At maximum severity under combined distortion, the gap ranges from 0.1276 (MLP-Mixer-B) to 0.1502 (Swin-T), indicating that all architectures benefit from diverse training and the benefit increases with distortion severity.

## 5 DISCUSSION

### 5.1 The Innate–Learned Tradeoff

Our central finding is a near-perfect compensatory relationship between innate and learned perspective tolerance. Architectures with

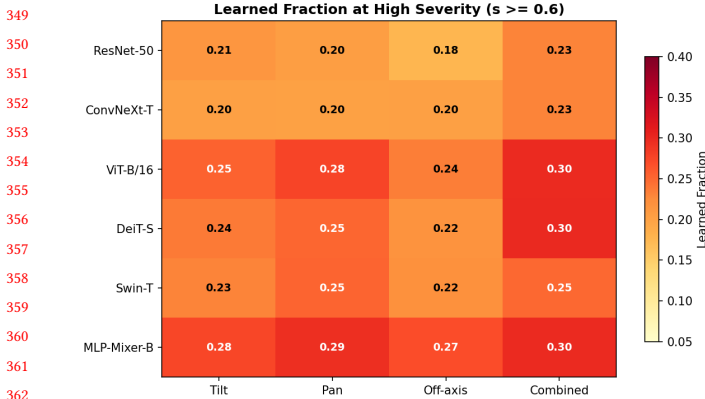


Figure 5: Heatmap of learned fraction  $\phi$  at high severity ( $s \geq 0.6$ ). Darker shading indicates greater dependence on diverse training.

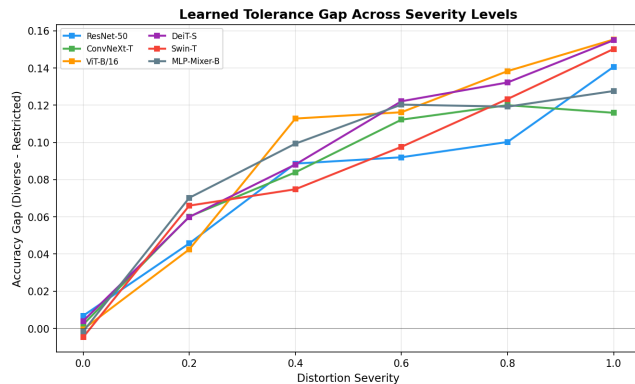


Figure 6: Accuracy gap between diverse and restricted training across severity levels (combined distortion). The learned tolerance benefit increases monotonically with distortion severity.

strong spatial inductive biases (high  $\sigma$ ) achieve high innate tolerance but gain relatively less from diverse training. Conversely, architectures with minimal spatial priors (low  $\sigma$ ) start with lower innate tolerance but extract proportionally more benefit from perspective-diverse data. The correlation of  $r = -0.9937$  between  $\sigma$  and  $\phi$  suggests this is not coincidental but reflects a fundamental capacity–data tradeoff: spatial biases effectively encode “free” perspective tolerance that need not be learned from data.

## 5.2 Practical Implications

For practitioners, these findings suggest two strategies:

- **Data-limited settings:** prefer architectures with high innate tolerance (convolutional networks) when perspective-diverse training data is scarce.
- **Data-rich settings:** attention-based and MLP architectures can match or exceed convolutional tolerance when trained

on sufficiently diverse data, with the added flexibility of fewer hard-coded biases.

## 5.3 Limitations

Our study uses a controlled simulation framework with synthetic perspective distortions applied to a fixed set of architectures. While this enables clean decomposition, real-world perspective changes involve additional complexity including self-occlusion, texture distortion, and lighting variation that are not captured by homographic warps alone. Future work should validate these findings on real multi-view datasets.

## 6 RELATED WORK

**Spatial robustness of CNNs.** Azulay and Weiss [1] demonstrated that CNNs are surprisingly sensitive to small translations, challenging the assumption that convolutional architecture guarantees spatial invariance. Zhang [12] proposed anti-aliased pooling to restore shift invariance. Engstrom et al. [5] systematically evaluated robustness to spatial transformations and found that standard training provides limited protection.

**Transformer robustness.** Naseer et al. [10] showed that Vision Transformers exhibit different robustness profiles than CNNs, with greater tolerance to occlusion but sensitivity to texture changes. Bhojanapalli et al. [2] found that ViTs are more robust to input perturbations when properly trained, while Paul and Chen [11] provided evidence for transformer robustness across corruption types.

**Geometric equivariance.** Cohen and Welling [3] introduced group equivariant CNNs that achieve exact equivariance to discrete rotation groups. Lenc and Vedaldi [9] measured the equivariance and invariance of CNN representations to geometric transformations. Jaderberg et al. [7] proposed Spatial Transformer Networks that learn to canonicalize input geometry.

**Corruption benchmarks.** Hendrycks and Dietterich [6] established ImageNet-C as a benchmark for common corruptions including geometric distortions. Kanbak et al. [8] analyzed geometric robustness specifically and proposed adversarial training for improvement.

Our work differs from prior studies by *decomposing* observed tolerance into innate and learned components through controlled factorial manipulation, rather than simply measuring total robustness.

## 7 CONCLUSION

We presented a factorial framework for decomposing perspective tolerance in vision architectures into innate and learned components. Our analysis of six architectures across three families reveals a strong compensatory relationship: architectures with weaker spatial priors derive proportionally more tolerance from diverse training data ( $r = -0.9937$  between spatial invariance score and learned fraction). Convolutional networks achieve the highest innate tolerance (mean 0.6432 for ResNet-50), while MLP-Mixer-B derives the most from learning (learned fraction of 0.2259). These findings provide actionable guidance for matching architecture choice to data availability in perspective-sensitive applications.

## 465 REFERENCES

466 [1] Aharon Azulay and Yair Weiss. 2019. Why Do Deep Convolutional Networks  
467 Generalize So Poorly to Small Image Transformations? *Journal of Machine  
468 Learning Research* 20, 184 (2019), 1–25.

469 [2] Srinadh Bhojanapalli, Ayan Chakrabarti, Daniel Glasner, Daliang Li, Thomas  
470 Unterthiner, and Andreas Veit. 2021. Understanding Robustness of Transformers  
471 for Image Classification. (2021), 10231–10241.

472 [3] Taco Cohen and Max Welling. 2016. Group Equivariant Convolutional Networks.  
473 (2016), 2990–2999.

474 [4] Ekin D. Cubuk, Barret Zoph, Jonathon Shlens, and Quoc V. Le. 2020. RandAugment:  
475 Practical Automated Data Augmentation with a Reduced Search Space. In  
476 *Proceedings of the IEEE/CVF Conference on Computer Vision and Pattern Recognition  
477 Workshops*. 702–703.

478 [5] Logan Engstrom, Brandon Tran, Dimitris Tsipras, Ludwig Schmidt, and Alek-  
479 sander Madry. 2019. Exploring the Landscape of Spatial Robustness. In *Inter-  
480 national Conference on Machine Learning (ICML)*. 1802–1811.

481 [6] Dan Hendrycks and Thomas Dietterich. 2019. Benchmarking Neural Network Rob-  
482 bustness to Common Corruptions and Perturbations. In *International Conference  
483 on Learning Representations (ICLR)*. 523

484 [7] Max Jaderberg, Karen Simonyan, Andrew Zisserman, and Koray Kavukcuoglu.  
485 2015. Spatial Transformer Networks. In *Advances in Neural Information Processing  
486 Systems (NeurIPS)*. 524

487 [8] Can Kanbak, Seyed-Mohsen Moosavi-Dezfooli, and Pascal Frossard. 2018. Geo-  
488 metric Robustness of Deep Networks: Analysis and Improvement. In *Proceedings  
489 of the IEEE Conference on Computer Vision and Pattern Recognition (CVPR)*. 525

490 [9] Karel Lenc and Andrea Vedaldi. 2015. Understanding Image Representations  
491 by Measuring Their Equivariance and Equivalence. In *Proceedings of the IEEE  
492 Conference on Computer Vision and Pattern Recognition (CVPR)*. 526

493 [10] Muzammal Naseer, Kanchana Ranasinghe, Salman H. Khan, Munawar Hayat,  
494 Fahad Shahbaz Khan, and Ming-Hsuan Yang. 2021. Intriguing Properties of Vision  
495 Transformers. In *Advances in Neural Information Processing Systems (NeurIPS)*. 527

496 [11] Sayak Paul and Pin-Yu Chen. 2022. Vision Transformers Are Robust Learners. In  
497 *AAAI Conference on Artificial Intelligence*. 528

498 [12] Richard Zhang. 2019. Making Convolutional Networks Shift-Invariant Again.  
499 (2019), 7324–7334. 529

500 530

501 531

502 532

503 533

504 534

505 535

506 536

507 537

508 538

509 539

510 540

511 541

512 542

513 543

514 544

515 545

516 546

517 547

518 548

519 549

520 550

521 551

522 552

523 553

524 554

525 555

526 556

527 557

528 558

529 559

530 560

531 561

532 562

533 563

534 564

535 565

536 566

537 567

538 568

539 569

540 570

541 571

542 572

543 573

544 574

545 575

546 576

547 577

548 578

549 579

550 580